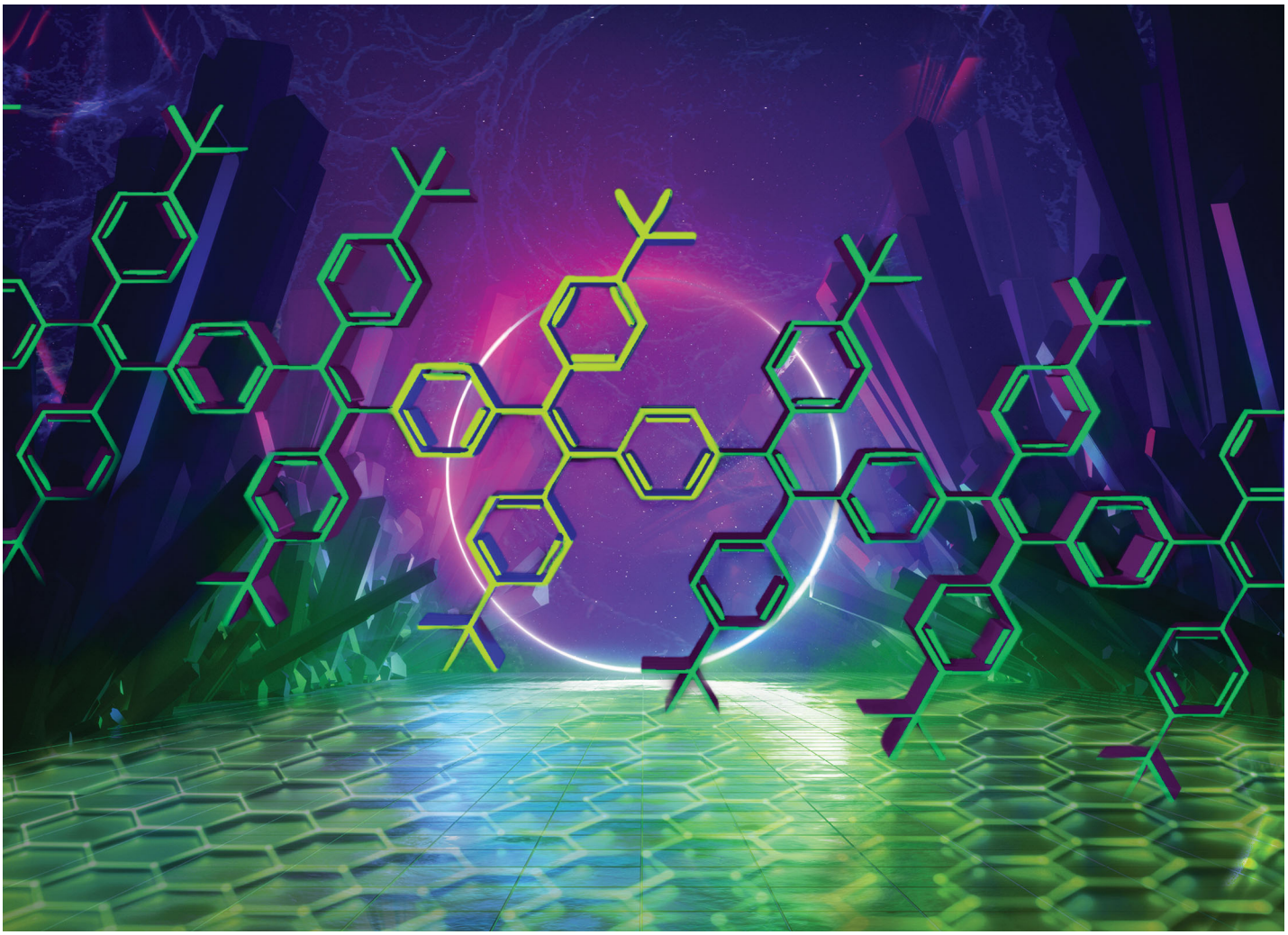

Showcasing research from the groups of Ullrich Scherf (University of Wuppertal, Germany) and Sérgio Seixas de Melo (University of Coimbra, Portugal)

Designing highly fluorescent, arylated poly(phenylene vinylene)s of intrinsic microporosity

Rational design of diarylated poly(phenylene vinylene) results in multifunctional, solution-processable polymer materials showing high fluorescence efficiency (ϕ_F up to 0.64) coupled to the occurrence of intrinsic microporosity (as so-called conjugated polymers of intrinsic microporosity, cPIMs; S_{BET} up to 417 $m^2\ g^{-1}$).

As featured in:

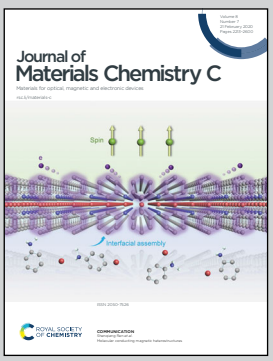

See Ullrich Scherf, J. Sérgio Seixas de Melo *et al.*, *J. Mater. Chem. C*, 2020, **8**, 2248.

ROYAL SOCIETY OF CHEMISTRY

rsc.li/materials-c

Registered charity number: 207890

Journal of Materials Chemistry C

ROYAL SOCIETY OF CHEMISTRY

PAPER

View Article Online
View Journal | View Issue

Cite this: J. Mater. Chem. C, 2020, 8, 2248

Designing highly fluorescent, arylated poly(phenylene vinylene)s of intrinsic microporosity†

Ana Clara B. Rodrigues, ‡[a] Isabell S. Geisler,‡[b] Patrick Klein, [b] João Pina, [a] Fabian J. H. Neuhaus,[b] Elke Dreher,[c] Christian W. Lehmann,[c] Ullrich Scherf *[b] and J. Sérgio Seixas de Melo *[a]

Received 12th November 2019,
Accepted 4th December 2019

DOI: 10.1039/c9tc06028f

rsc.li/materials-c

Three new polymers containing tetraphenylethylene and diphenyl-dinaphthylethylene cores and their corresponding monomeric model compounds were synthesized and fully characterized aiming to investigate their photoluminescence efficiency, microporosity and Brunauer–Emmett–Teller-derived surface areas (S_{BET}). Comprehensive photophysical characterization was undertaken in the solid state (powder and thin films), in tetrahydrofuran (THF) solution and in mixtures of "good" and "poor" solvent to induce aggregation (THF:water mixtures). Aggregation induced emission (AIE) was found for the *tert*-butyl-**TPE** monomer and polymer and diphenyl-dinaphthylethylene monomer with the increase of the water amount in THF:water mixtures and in the solid state. The *tert*-butyl substituted **TPE** derivatives display the highest fluorescence quantum yield (ϕ_F) values: 0.14 to 0.30 (in powder) and 0.46 to 0.64 in thin films. In contrast, with the diphenyl-dinaphthylethylene (*meta* and *para*-phenylene) polymers aggregation caused quenching (ACQ) occurs in THF:water mixtures ($\phi_F \leq 0.011$) and in the solid state ($\phi_F \leq 0.012$). The microporosity of the soluble conjugated polymers as potential conjugated polymers of intrinsic microporosity (cPIMs) was further investigated. The S_{BET} of the polymers were related to their optical properties. The polymers show an attractive combination of high S_{BET} surface area (417 $m^2\ g^{-1}$) and the occurrence of distinct AIE effects for the *tert*-butyl-**TPE** polymer while the diphenyl-dinaphthylethylene polymers do not exhibit microporosity ($S_{BET} \leq 17\ m^2\ g^{-1}$) and show ACQ behavior.

Introduction

Aggregation induced emission (AIE, or even aggregation induced enhanced emission, AIEE) corresponds to the description of the luminescence phenomenon in which the luminescence efficiency of a luminogen is increased upon its aggregation.[1] The most accepted mechanism for the occurrence of AIE is through a restriction of intramolecular motions (RIM), including rotations and vibrations, that would deactivate non-radiatively the excited state of the luminogens.[2] This phenomenon occurs in some luminogens in contrast to aggregation caused quenching (ACQ) commonly described for traditional fluorophores in which the π–π-stacking of the molecules at high concentration or in the solid state leads to the formation of H-aggregates, which decreases the emission efficiency.[3] Typically, low molecular weight AIE chromophores possess a propeller-shaped structure with rotatable peripheral phenyl rings (rotors),[4] such as 1,1,2,3,4,5-hexaphenylsilole (HPS),[5] 2,3,3-triphenylacrylonitrile (TPAN)[6] and 1,1,2,2,-tetraphenylethylene (**TPE**).[7] **TPE** derivatives have demonstrated a wide range of applications in optoelectronic devices,[8–10] bioimaging,[11] biosensors,[12] *etc.* due to their AIE properties.

TPE-based conjugated polymers – poly(arylene-diphenylvinylenes) – have been known since the 1960s.[13] Soluble, high molecular weight poly-**TPE**s (M_n 10–40 kDa) can be made in reductive polyolefinations of aromatic, bisgeminal tetrachlorides as diketone derivatives with Cr_2ac_4 or $Co_2(CO)_8$ as reducing agents[14–16] or in carbonyl polyolefinations after McMurry with $TiCl_3/LiAlH_4$.[17] Some of them show distinct AIE properties

[a] CQC, Department of Chemistry, University of Coimbra, P3004-535 Coimbra, Portugal. E-mail: sseixas@ci.uc.pt
[b] Bergische Universitat Wuppertal, Macromolecular Chemistry Group (buwmakro) and Institute for Polymer Technology, Gauss-Str. 20, D-42119 Wuppertal, Germany. E-mail: scherf@uni-wuppertal.de
[c] Max-Planck-Institut für Kohlenforschung, Kaiser-Wilhelm-Platz 1, D-45470 Mülheim an der Ruhr, Germany

† Electronic supplementary information (ESI) available: Detailed synthesis and structural characterization of model compounds and polymers; crystal data and structure refinement of monomers; nitrogen gas adsorption and desorption isotherms of polymers and their BET surface area fits and room temperature fluorescence decays for Poly-*t*-Bu. CCDC 1961126 and 1961127. For ESI and crystallographic data in CIF or other electronic format see DOI: 10.1039/c9tc06028f

‡ These authors contributed equally to the work.

leading to high solid state photoluminescence quantum yields of >70% for some of the poly-**TPE**s.[4,18] Since 2011,[19,20] the easily functionalized four phenyl rings of the **TPE** unit were combined with a variety of reactive groups in construction of **TPE**-based polymers with inherent porosity.[21] The development of microporous organic polymers (MOPs) with very high surface area is an active field of current research,[22] with high potential in a variety of applications[4,23–26] such as energy storage, light harvesting, catalysis and sensing of hazardous chemicals and explosives. Several classes of MOPs, such as amorphous hyper-cross-linked polymers (HCPs), polymers of intrinsic microporosity (PIMs), and conjugated microporous polymers (CMPs), have been reported.[27] CMPs are also potential fluorescent materials due to their extended conjugated frameworks and tunable optoelectronic properties.[28]

In this work, two types of poly(1,4-phenylene-diarylvinylene)s with 4-*tert*-butylphenyl or naphthyl as aryl substituents at the vinylene units as well as the corresponding poly(1,3-phenylene-dinaphthylvinylene) are investigated for their photophysical properties in tetrahydrofuran (THF) and THF:water mixtures (a mixture of a ''good solvent'', THF, and water, a ''poor solvent'' to induce the formation of aggregates) as well as in the solid state (powder and films) for studying the effect of aggregation on the photoluminescence efficiency. The results are further rationalized with investigations on monomeric model monomer compounds and with the parent **TPE** molecule under the same conditions to also elucidate the effect of the substituent and polymerization on the photophysical properties of these compounds. Furthermore, the porosity of these new **TPE**-based polymers is also investigated.

Experimental section

Materials

Most chemicals were purchased from Sigma-Aldrich, Fischer Scientific or TCI and used without further purification, unless described otherwise. For the photophysical studies, the solutions were prepared with solvents of spectroscopic grade or equivalent: tetrahydrofuran (THF, Uvasol Merck), analytical grade chloroform (Fischer Chemical) or deionized water (18.2 MΩ cm at 25 °C, Milli-Q, Millipore).

Synthesis and structural characterization of the model compounds and polymers

All reactions were carried out under an argon atmosphere using flame dried glassware. The detailed synthetic procedure and structural characterization are provided in the ESI.† NMR spectra were recorded on a Bruker AVANCE 400 or AVANCE III 600. APCI (Atmospheric Pressure Chemical Ionization) and ESI (electrospray ionisation) mass spectra were obtained on a Bruker Daltronik micrOTOF system. Gel permeation chromatography (GPC) measurements were carried out on a PSS/Agilent SECurity GPC system equipped with polystyrene gel columns using chloroform or THF as the eluent. Nitrogen adsorption–desorption isotherms were recorded on a BEL Japan Inc Belsorp-max system at 77 K. The surface areas were calculated using the BET model in the pressure range p/p_0 from 0.05–0.25. All samples were degassed offline at >100 °C for 16 hours under a vacuum. Single crystal X-ray structures were obtained on a Bruker-AXS Kappa Mach3 APEX-II-diffractometer with a FR591 rotating anode, equipped with graded multilayer optics emitting copper radiation (1.54178 Å), and measured at 100 K. For structure solution and refinement, the SHELX-package[29,30] was used as integrated in Olex2.[31]

Solutions and film preparation

An appropriate amount of powder of each compound was diluted in THF to prepare a stock solution with an optical density of 1.0 at the excitation wavelength used for the experiments. Then, 100 μL of the stock solution was then diluted with the proper amount of THF or THF:water mixture to obtain the desired water fraction (f_W = 0–95%, v/v) in 2 mL of final volume.

Thin films from the compounds were obtained with a desktop precision spin-coating system, model P6700 series from Speedline Technologies, as described elsewhere.[32] Briefly, thin films from the samples were obtained by deposition of *ca.* 50 μL from a solution of the compounds onto a circular sapphire substrate (10 mm diameter) followed by spin-coating (2500 rpm) in a nitrogen-saturated atmosphere (2 psi). The solutions for spin-coating were prepared by adding 2 mg of the samples to 200 μL of chloroform solution, with stirring, at environment temperature, overnight. 15 mg of Zeonex® was added to the chloroform solution of the model compounds, **TPE**, **Mono-*t*-Bu** and **Mono-Np**, as a polymeric matrix to obtain thin films of these samples.

Steady state and time-resolved fluorescence measurements

The absorption spectra were recorded using Shimadzu UV-2450 or Agilent Cary 5000 UV-vis-NIR spectrometers. Absorption spectra of the transparent thin films were obtained in absorption mode using a clean sapphire substrate as the reference sample. The absorption spectra of the amorphous powder samples were recorded by collecting diffuse reflectance using a Cary 5000 DRA (an integrating sphere accessory with detection in the 200–2500 nm range). Background correction was performed by collecting the baseline with 100% and 0% reflectance (using a polytetrafluoroethylene, PTFE, reference sample and a blocked beam, respectively) prior to the determination of the spectra of the solid samples. Conversion to absorption was performed assuming the Kubelka–Munk function, $F(R)$.[33]

Fluorescence spectroscopic studies were performed using a Horiba-Jobin-Yvon Fluorolog 3-22 spectrofluorimeter. The fluorescence quantum yields (ϕ_F) of all compounds, in solution or in the solid state, were measured using the absolute method with a Hamamatsu Quantaurus QY absolute photoluminescence quantum yield spectrometer, model C11347 (integrating sphere). A clean sapphire substrate was used as a reference for the ϕ_F measurements of solid-state thin films.

Fluorescence decays were measured using a home-built Time-Correlated Single Photon Counting (TCSPC) apparatus described previously.[32] An IBH nanoLED (339 nm, 1.0 kHz) was used as the excitation source. The fluorescence decays and

the instrumental response function (IRF) were collected using 1024 channels on a time scale of up to 48.8 ps per channel; alternate measurements (500 counts) of the pulse profile at the excitation wavelength and the sample emission were performed until 3000 counts at the maximum were reached. Deconvolution of the fluorescence decay curves was performed using the modulation function method in the SAND program, as previously described.[34]

Results and discussion

Synthesis and physical characterization of the polymers and monomeric model compounds

The structures and acronyms of the investigated compounds are depicted in Scheme 1.

Three new polymers comprising tetraphenylethylene and diphenyl-dinaphthylethylene backbones together with their corresponding monomeric analogues were synthesized according to the general strategic methodology described in Scheme 2. These polymers were inspired by the well-known aggregation induced emission, AIE, luminogen, 1,1,2,2-tetraphenylethylene (**TPE**).[1,7,24,35–37]

All polymers were synthesized *via* reductive polyolefinations of aromatic, bisgeminal tetrachlorides following a procedure initially described by Hörhold and co-workers in the 1970s.[14,38,39] In contrast to the original procedure dicobalt octacarbonyl was used as a condensing agent, a variation of Hörhold's method developed by us in the 1990s.[15] The required tetrachlorides were generated starting from the commercially available tere- or isophthaloyl chlorides in two steps (Scheme 2a). In the first step diketones were synthesized following a modified Friedel–Crafts-acylation procedure using tere-/isophthaloyl chloride and *tert*-butylbenzene or naphthalene.[40,41] Next, the bisgeminal tetrachlorides were obtained by reaction of the diketones with phosphorous pentachloride as described by Hörhold *et al.*[14,38]

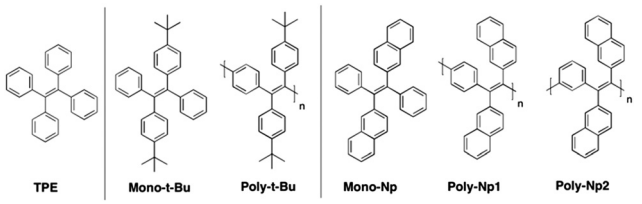

Scheme 1 Representative structures and acronyms of the investigated polymers, and **TPE** and *tert*-butylbenzyl and naphthyl monomeric model compounds.

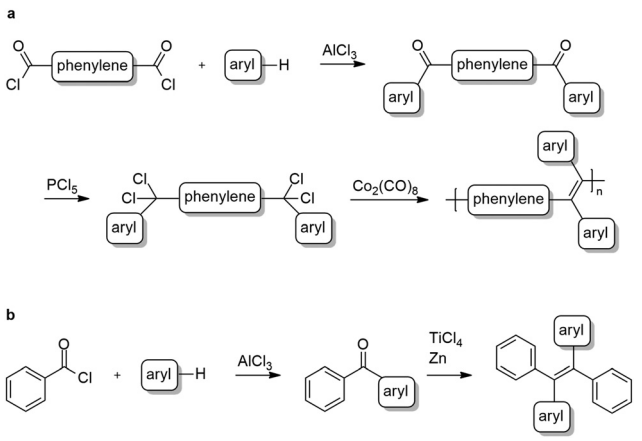

Scheme 2 General synthesis of polymers (a) and phenyl-terminated monomers (b).

The monomeric model compounds were prepared in a two-step synthesis. First benzoyl chloride and naphthalene or *tert*-butylbenzene were converted to the corresponding diarylketones in a Friedel–Crafts-acylation protocol[42] (Scheme 2b). In the case of naphthalene, the resulting mixture of 1-benzoylnaphthalene and 2-benzoylnaphtalene was separated using flash column chromatography. In the second step the desired tetraarylethylenes were obtained by reductive coupling of the ketones using titanium tetrachloride and zinc.[43] The 1 : 1 mixtures of *E*/*Z*-isomers in the products (as determined from the ^{1}H-NMR spectrum) were separated by recrystallization.

The average molecular weight, $\bar{M}_n$, weight average molecular weight, $\bar{M}_w$, and polydispersity (PD) values of the polymers are listed in Table 1. Based on the $\bar{M}_n$ values the degrees of polymerization (DP) have been calculated. The two naphthyl-substituted polymers, **Poly-Np1** and **Poly-Np2**, can be assigned to the same model compound, **Mono-Np**; **Poly-Np1** incorporates *para*-phenylene main chain linker units, while **Poly-Np2** contains *meta*-phenylene main chain units (Scheme 1). **Poly-Np1** and **Poly-Np2** display reduced molecular weights, most probably caused by the increased steric demand coupled with decreased polydispersity (PD) values. Table 1 also lists the BET-based surface areas (S_{BET}) of the solid polymer powders extracted from nitrogen sorption/desorption isotherms (Fig. SI1 and SI2, ESI†). Obviously, only **Poly-*t*-Bu** exhibits intrinsic microporosity with a high S_{BET} surface area of up to 417 $m^2 g^{-1}$ as a so-called conjugated polymer of intrinsic microporosity (cPIM).[23]

The investigated phenyl-terminated monomeric model compounds, **Mono-*t*-Bu** and **Mono-Np**, are both of E-configuration as determined by single crystal X-ray crystallography (see Fig. 1). In the crystalline state, **Mono-*t*-Bu** adopts a propeller like conformation with dihedral angles between the plane subtended by the central double bond and the phenyl rings of 52.3° and 55.9°. The ring planes of the two *tert*-butylphenyl groups are rotated slightly less, by 38.8° and 41.1°. The molecular conformation of **Mono-Np** is similar to that of **Mono-*t*-Bu**. The molecule is located on a crystallographic twofold axis and consequently only one independent dihedral angle between the two phenyl rings and the olefinic bond exists.

Table 1 Physical characteristics of the polymers investigated[a]

Compound	$\bar{M}_n$ (g mol^{-1})	$\bar{M}_w$ (g mol^{-1})	PD	DP	S_{BET} ($m^2 g^{-1}$)
Poly-*t*-Bu	29 300	164 000	5.62	80	417
Poly-Np1	11 600	17 800	1.54	33	14
Poly-Np2	5300	9400	1.77	15	17

[a] Mean and weight average molecular weights ($\bar{M}_n$ and $\bar{M}_w$), polydispersity (PD) and the degree of polymerization (DP) calculated based on the average molecular weight ($\bar{M}_n$) and BET-derived surface area (S_{BET}).

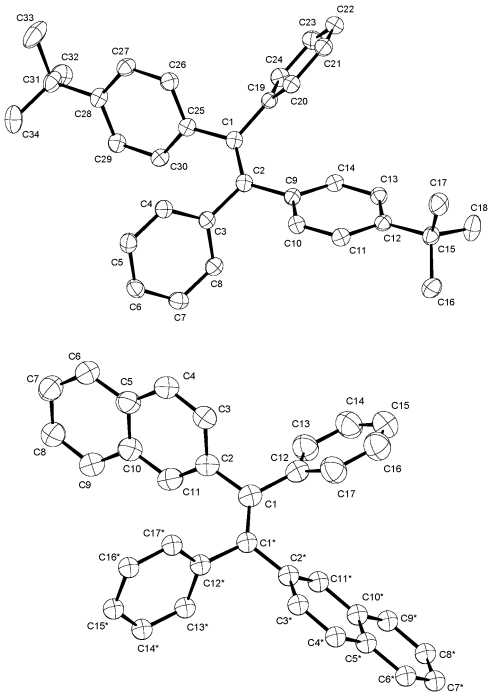

Fig. 1 Molecular structures of the phenyl-terminated monomeric model compounds, **Mono-*t*-Bu** and **Mono-Np**, determined by single crystal X-ray crystallography.

This amounts to 56.2°. The same symmetry restriction holds for the naphthyl rings, which are rotated by 53.3° against the plane of the double bond. While the molecular conformations of the two propeller shaped molecules are similar, a marked difference is observed regarding the intermolecular interactions. **Mono-*t*-Bu** does not form π–π interactions, either between the *tert*-butyl rings or the phenyl rings. In contrast, **Mono-Np** exhibits π-stacking between the naphthyl rings. The shortest C–C contact between the rings is 3.32 Å and slightly shorter than in graphite (Fig. 2). The distance between the centroids of the overlapping halves of the naphthyl rings is 4.8 Å, indicating ring slippage and reduced overlap of the π-systems. However, the π-stacking is not limited to pairs of molecules but extends infinitely through the crystal along the *c*-axis. Also, the observed differences in the surface area values of the polymers should result from the different packing behaviour of the 4-*tert*-butylphenyl *vs.* naphthyl side groups. Indeed, while the naphthyl side groups tend to aggregate (π-stack) with neighbouring side groups in the solid state, the 4-*tert*-butylphenyl groups with their bulky *tert*-butyl substituents create free volume and microporosity (please see also the discussion of the X-ray crystal structures of the monomers).

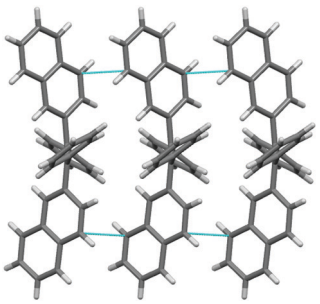

Fig. 2 View of the crystal packing of **Mono-Np**, showing short Cπ–Cπ interactions (in cyan) parallel to the *c*-axis.

Electronic spectral data

The photophysical properties of the polymers and model compounds, **TPE** and phenyl-terminated monomers, were investigated in the solid state (amorphous powders and thin films), in tetrahydrofuran (THF) solution and in mixtures of good and poor solvent (THF:water mixtures) to evaluate the effect of aggregation on the fluorescence emission efficiency.

Fig. 3 presents the absorption and fluorescence emission spectra of the polymers and model compounds in the solid-state (powder and thin films) and in THF solutions. The spectroscopic data in Fig. 3 are designed and structured in order to compare the polymer with the respective monomeric model compound plus the model AIGen, **TPE**.

The same wavelength scale is presented for all the compounds, which further allows a direct comparison between the two types of polymers.

The absorption and emission spectra of the investigated compounds in the amorphous powders are red-shifted and broader than in THF solution, indicating an extent of conjugation through intermolecular packing in the solid state (see Fig. 3 and Table 2). Additional observation of the spectral behavior shows that there is a good match between the solution absorption band profiles and those obtained in thin films for the polymers and monomers (although with a different maximum, Table 2).

Observation of Fig. 3 and Table 2 shows that the emission spectra of the polymers are red-shifted relative to the monomeric model compounds, emitting in the visible green region of the light spectrum: in solution, the emission maxima correspond to 530 nm, for **Poly-*t*-Bu**, and 545 nm and 518 nm for **Poly-Np1** and

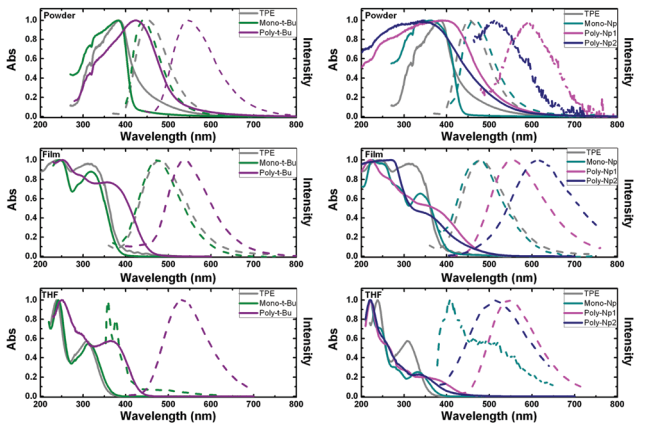

Fig. 3 Normalized absorption and emission spectra for the compounds in powder and thin films (*i.e.*, in a solid environment) and in THF solution. For better comparison the polymers together with the corresponding monomer are presented the same graph. Solid line: normalized absorption spectra; dashed line: normalized emission spectra. For comparison, the **TPE** absorption and emission spectra are shown (grey lines).

Table 2 Room temperature spectroscopic data (absorption and fluorescence emission maxima together with Stokes shift, Δ_{SS}) for the polymers and model compounds in THF, amorphous powders and thin films

Compound	Medium	λ^{abs} (nm)	λ^{em} (nm)	Δ_{SS} (cm^{-1})
TPE	Powder[a]	381	454	4220
	Film[b]	243/312	482	11 304
	THF[a]	238/308	—	—
Mono-*t*-Bu	Powder	382	441	3052
	Film[b]	245/320	473	10 108
	THF	242/314	358, 490	3914
Poly-*t*-Bu	Powder	421	546	5438
	Film	252/355	537	9547
	THF	250/366	530	8454
Mono-Np	Powder	362	468	6257
	Film[b]	226/337	479	8797
	THF	220/334	407, 490 (sh)	5370
Poly-Np1	Powder	391	590	8626
	Film	222/351	553	10 407
	THF	222/343	545	10 806
Poly-Np2	Powder	346	511	9332
	Film	268/348	611	12 369
	THF	221/335	518	10 546

[a] Data from ref. 44. [b] Prepared using Zeonex® as a polymeric matrix.

Table 3 Room temperature fluorescence quantum yields (ϕ_F) for the investigated model compounds and polymers in different media

	THF	90W : 10 THF	Powder	Film
TPE	0.003	0.25	0.23[a]	0.26[b]
Mono-*t*-Bu	0.024	0.20	0.14	0.46[b]
Poly-*t*-Bu	0.046	0.62	0.30	0.64
Mono-Np	0.003	0.043	0.14	0.12[b]
Poly-Np1	0.028	0.011	0.012	0.010
Poly-Np2	0.008	0.003	0.004	0.002[c]

[a] Data from ref. 44. [b] Prepared using Zeonex® as a polymeric matrix. [c] ϕ_F determined by comparison with the emission area of the **Poly-Np1** film, with the same absorption at the excitation wavelength.

Poly-Np2, respectively. In films, **Poly-Np2** presents the highest emission wavelength found for the studied compound, with a maximum at 611 nm (Table 2). Generally, the polymers also have higher Stokes shifts (Δ_{SS}) when compared to their respective monomers, in the same medium. Since charge transfer bands cannot occur in these polymers this behavior points to the adoption of different conformations in the ground- and excited-state of the polymers (probably adopting a more planar conformation in the excited-state, which can lead to an extended degree of conjugation). The more extended nature of the π-conjugation in **Poly-Np1** compared to **Poly-Np2** in THF solution may be explained by the fact that the *para*-phenylene units in **Poly-Np1** formally allow extended π-conjugation along the main chain (not much due to its strongly distorted conformation), while in **Poly-Np2**, the *meta*-phenylene main chain units act now as effective conjugation barriers. This is further reflected in the differences observed in the solution absorption and emission (solvent:THF) spectra (Fig. 3, bottom right hand panel). In contrast with these results, a different behavior is found in thin films (Fig. 3, middle right hand panel) where the fluorescence spectrum of **Poly-Np2** is red-shifted when compared to **Poly-Np1**. While the THF solution and thin film emission maxima of **Poly-Np1** are quite similar (545 nm in THF solution *vs.* 553 nm in the thin film), **Poly-Np2** shows a distinctly red-shifted PL maximum when compared to the solution value (611 nm in the thin film *vs.* 518 nm for the THF solution). This finding may be explained by increased side chain aggregation (and AQC) in **Poly-Np2** with the aggregate emission as the dominating feature. This explanation is supported by the reduced thin film ϕ_F for **Poly-Np2** (PLQY: 0.02 for **Poly-Np1** *vs.* 0.001 for **Poly-Np2**, which will be further discussed in the next section on Table 3).

Upon going from the monomeric model compound, **Mono-*t*-Bu**, to the polymer **Poly-*t*-Bu** a significant red shift of the absorption spectra is observed (39 nm in powder, 35 nm in film and 52 nm in THF). The same is not found for the **Poly-Np** polymers in THF and thin films where a small red shift is observed when compared to **Mono-Np** (see Table 2). This shows that the chromophoric unit is in these polymers limited to the monomeric counterpart.

In the case of **Mono-Np** the two bands at maxima 407 nm and 498 nm (Fig. 3, right hand bottom panel) indicate the coexistence of monomer and aggregate species. This is further complemented with a concentration dependence study in Fig. SI3 (ESI†).

It is also worth noting that in the solid state (powder and thin films) the investigated phenyl-terminated monomers retain the electronic spectral absorption features and maxima found for **TPE** (Fig. 3). On going to solution (THF), although red-shifted (~6 nm for **Mono-*t*-Bu** and ~26 nm for **Mono-Np**, see Table 2), similar broad absorption bands are observed for the monomeric model compounds when compared with **TPE**. The higher bathochromic shift found for **Mono-Np** can be attributed to the increase in the conjugation segment promoted by the naphthyl moieties when compared with the phenyl units in **TPE**.[37]

Clearly contrasting with the behavior found for **TPE** in good solvents, where fluorescence emission is almost negligible (with ϕ_F values of 0.002 or 0.0024 and of 0.003 in Table 3),[37,45,46] the phenyl-terminated monomeric model compounds, **Mono-*t*-Bu** and **Mono-Np**, display fluorescence both in solution and in the solid state (Fig. 3 and Table 3). Indeed, **TPE** itself fluoresces when aggregated in solution[37,47] or in the solid state (Fig. 3), *i.e.*, when restriction of intramolecular rotation (RIR) occurs, thus hindering the excited state radiationless processes.

In THF solution, when **TPE** is compared with the *tert*-butyl-**TPE** (**Mono-*t*-Bu**) derivative, the absorption spectra almost totally match and the emission is absent in **TPE**. However, in the case of **Mono-*t*-Bu**, the emission spectrum presents two bands: a vibronically resolved band with a maximum at ~358 nm (corresponding to the monomer) and a second broad band with a maximum at ~490 nm corresponding to the emission of the aggregate. This last band increases and red-shifts with the addition of water (Fig. 4). Moreover the ϕ_F value of **Mono-*t*-Bu** in THF is one order of magnitude higher than that of **TPE** (Table 3).

Although the emission spectra of the model compounds **Mono-*t*-Bu** and **Mono-Np** in films quite overlap with that of **TPE**, in powder the emission of **Mono-*t*-Bu** is blue-shifted when compared to **TPE**, with emission maxima of 441 nm and

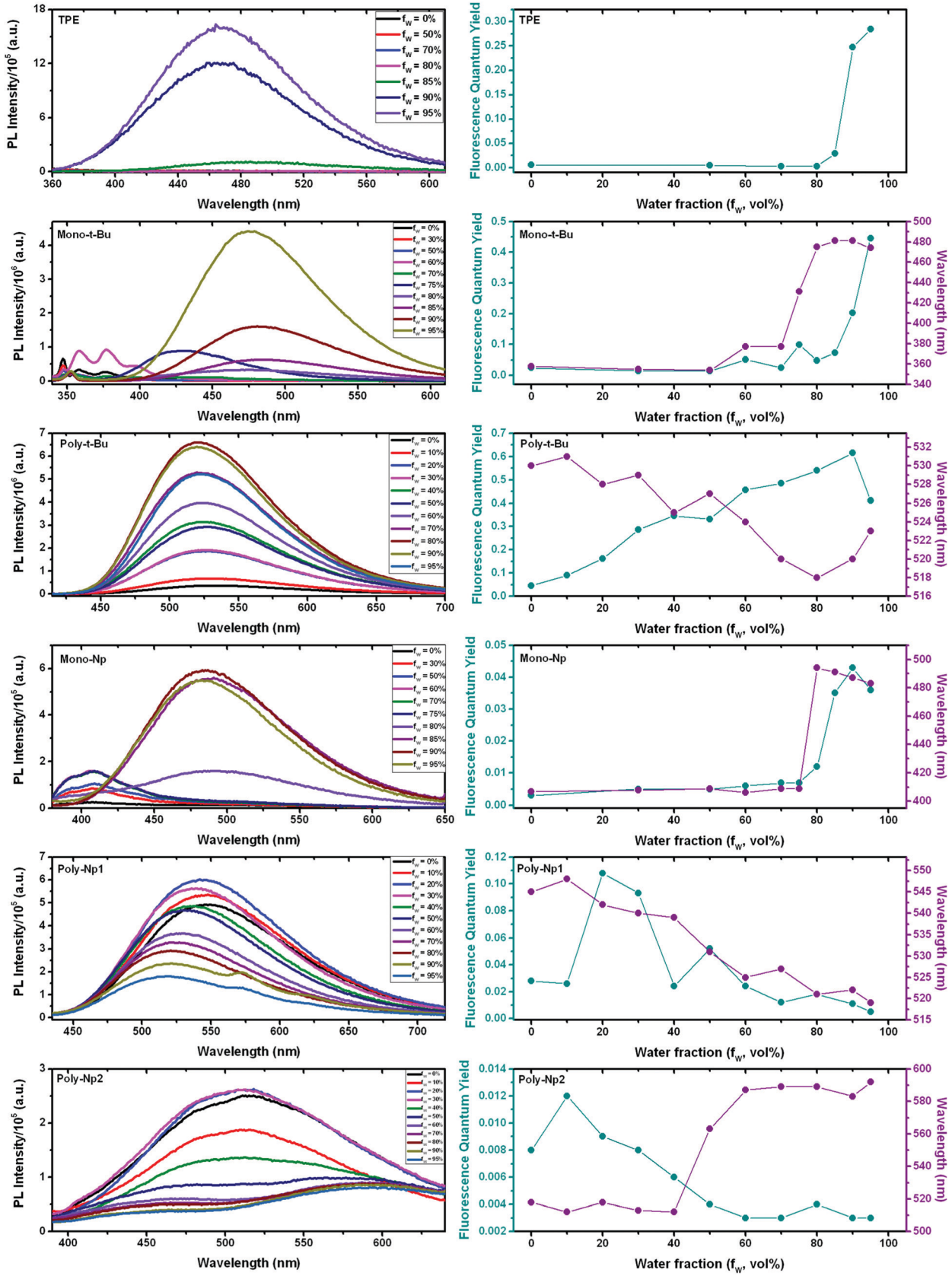

Fig. 4 Room temperature fluorescence emission (photoluminescence, PL) spectra for the model compounds (**TPE**, **Mono-*t*-Bu** and **Mono-Np**) and polymers (**Poly-*t*-Bu**, **Poly-Np1** and **Poly-Np2**) in THF:water mixtures and their respective correlation of the fluorescence quantum yield and emission maxima with increasing water fraction, f_W = 0–95%. The lines in the right hand panels are just meant to be a guide to the eye.

454 nm for **Mono-*t*-Bu** and **TPE**, respectively (Fig. 3 and Table 2). In the case of **Mono-Np** and again compared with **TPE**, there is now a red-shift of the emission maximum of 14 nm (Table 2). For the latter monomer the observed red-shift together with the increase in the fluorescence quantum yield on going from solution to the solid state gives support to the formation of J-aggregates.[48]

Aggregation induced emission (AIE) studies

To further explore the occurrence of AIE in the investigated compounds, the emission behavior was studied in THF:water mixtures (Fig. 4). **TPE** blue emission is only visible in high water content, either in acetonitrile:water[7] or in THF:water mixtures.[49] The broad emission band associated with this emissive aggregate, centered at *ca.* 470 nm, becomes detectable at a water fraction (f_W) $\geq$ 85%.

Enhancing the steric effect is an efficient means to activate the restriction of intramolecular motion (RIM) process,[47] which is considered one of the possible mechanisms to explain the AIE phenomenon.[50] The phenyl rings in **TPE** have been substituted with multiple methyl groups at the *o*-positions to examine how the intramolecular steric effects affect its photophysical properties and AIE properties.[46] It was shown that the sterically crowded **TPE** derivative with four methyl groups loses its AIE activity, directly validating the RIM hypothesis.[51] However, it is expected that the *t*-Bu groups substituted in the *p*-position of the benzyl rings of **TPE** should enhance the steric effect and not affect the rotation of the aromatic rotors; therefore, the **Mono-*t*-Bu** monomer should present AIE properties. To verify this hypothesis, the emission spectra and fluorescence quantum yields (ϕ_F) for **Mono-*t*-Bu** were obtained in THF:water mixtures. Naphthalene-substituted ethenes, such as **Mono-Np**, are AIE-active luminogens.[37]

The spectral behavior of the investigated model compounds and polymers in THF:water mixtures, aiming to observe the presence of and to quantify the AIE effect, is shown in Fig. 4 and Table 3. From Fig. 4, it can be seen that **Mono-*t*-Bu** presents a structured emission spectrum in THF:water mixtures up to f_W = 60% (f_W: water:THF fraction, v/v), increasing in intensity with the addition of water. From $f_W \geq 70\%$ on, the emission maximum for **Mono-*t*-Bu** red-shifts and the ϕ_F value increases with the addition of water, up to ϕ_F = 0.2 for f_W = 90%, *i.e.*, $\sim$1 order of magnitude higher than in pure THF (Table 3).

Mono-Np shows a similar behavior (to that found for **Mono-*t*-Bu**), *i.e.*, a vibronically resolved spectrum up to f_W = 60% and a red-shifted emission band, followed by an increase in the ϕ_F values for $f_W \geq 70\%$. This observation is likely due to the formation of J-aggregates in the two phenyl-terminated monomers. Indeed, although the presence of the naphthalene rings could favor π–π interactions, leading to the formation of H-aggregates and consequently to aggregation caused quenching (ACQ), the opposite behavior was found.

The ϕ_F values for **TPE** and **Mono-Np** in films have been previously reported as 0.49 and 0.30, respectively.[37] Our values in Table 3 are 0.24 (**TPE**) and 0.46 (**Mono-*t*-Bu**), while for **TPE** in a THF:water mixture ϕ_F = 0.14 for f_W = 95% was previously reported[46] in comparison with our ϕ_F of 0.25 (for f_W = 90%). The values obtained in this study are slightly different from those reported previously in films. This is likely because the photophysical properties are intrinsically dependent on the morphological properties of the films. Indeed, and exemplifying this, the ϕ_F of **TPE** in powder was described as 24.1%,[52] found to be in good agreement with the value previously obtained by us (23%)[44] with the same equipment that was used to perform all the ϕ_F measurements.

Usually, when AIEgens, such as **TPE** and its derivatives, are chemically incorporated into polymeric structures, polymers with AIE characteristics could be obtained.[32,36,53] Thus, it was anticipated that **Poly-*t*-Bu** and **Poly-Np1** and **Poly-Np2**, whose monomeric model compounds are AIE active, would also maintain AIE properties. Although **Poly-*t*-Bu** presents an increase of fluorescence quantum yield upon the increase of the water fraction, the fluorescence of the naphthyl polymers is quenched with the addition of water in THF:water mixtures. Indeed, as can be seen from Fig. 2 **Poly-Np1** and **Poly-Np2** present ACQ. Moreover, as shown in Table 3, the ϕ_F of **Poly-Np2** is smaller than **Poly-Np1** in solution and the solid state and when compared at the same f_W in THF:water mixtures. The ACQ behaviour of **Poly-Np1,2** may be caused by the stacking tendency of the naphthyl groups, leading to the formation of H-type aggregates. This is supported by the observed intermolecular π-interactions of the naphthyl substituents in the single crystal structure of **Mono-Np**.

In the solid state, the highest photoluminescence efficiency was obtained for **Poly-*t*-Bu**, with ϕ_F = 64% in film – an increase of *ca.* 14× when compared to THF and higher than **TPE** and **Mono-*t*-Bu** – and when aggregated in THF:water mixtures it shows a value of ϕ_F = 62% for f_W = 90%.

The combination of **TPE** and carbazole groups also generated porous organic polymers with higher S_{BET} area, varying from 472 to 2200 $m^2\ g^{-1}$,[24,25,54] with fluorescence quantum yields of up to 40% in films[55] (see also Table SI5, ESI,† for a literature review of S_{BET} and fluorescence quantum yield values for porous **TPE** based polymers). In our set of **TPE** derived polymers, a new compound with moderate surface area (412 $m^2\ g^{-1}$), but higher fluorescence quantum yields (64% in spin coated films), is described.

Time resolved fluorescence decays were also obtained in order to gain further insight into the aggregate formation, *i.e.*, AIE in **Poly-*t*-Bu**. The fluorescence decays of **Poly-*t*-Bu** in THF and THF:water mixtures were found to be well fitted with a bi-exponential decay law (Fig. SI4, ESI†), thus indicating the presence of two emitting species in the aggregate region (λ_{em} = 525 nm). This possibly indicates that the emissive aggregate results from two main conformers with different contributions. Indeed, the fractional contribution (C_i), in Table 4, of each species is given by the following equation[56]

$$C_i(\%) = \frac{a_i\tau_i}{\sum_{i=1}^{n} a_i\tau_i} \times 100 \quad (1)$$

where n stands for the number of exponential terms and a_i the contribution of each exponential term at t = 0 and τ_i is the associated decay time.

Table 4 Room temperature fluorescence quantum yields (ϕ_F) and lifetimes[a] (τ) for **Poly-*t*-Bu** in selected THF:water mixtures. Also present are the associated pre-exponential values (a_i) and fractional contribution of each decay time (%C_i) and the chi-square values (χ^2) for the judgment of the quality of the fits. Radiative (k_F) and radiationless rate (k_{NR}) constants associated with the second decay component (τ_2) are also presented

Solvent	a_1	τ_1 (ns)	a_2	τ_2 (ns)	χ^2	ϕ_F	%C_1	%C_2	k_F[b] (ns^{-1})	k_{NR}[c] (ns^{-1})
100% THF : 0% water	0.947	0.23	0.053	1.45	1.01	0.046	73.9	26.1	0.032	0.658
80% THF : 20% water	0.768	0.5	0.232	1.87	1.29	0.161	47.0	53.0	0.086	0.449
50% THF : 50% water	0.692	0.78	0.308	2.36	1.27	0.332	42.6	57.4	0.141	0.283
30% THF : 70% water	0.627	0.98	0.373	2.74	1.35	0.485	37.5	62.5	0.177	0.188
10% THF : 90% water	0.601	1.23	0.399	3.3	1.05	0.612	36.0	64.0	0.185	0.118

[a] Experimental conditions: nanoLed λ^{ex} = 339 nm; λ^{em} = 525 nm; 48.1 ps per channel, 3k counts. [b] $k_F = \frac{\phi_F}{\tau_F}$. [c] $k_{NR} = \frac{(1-\phi_F)}{\tau_F}$.

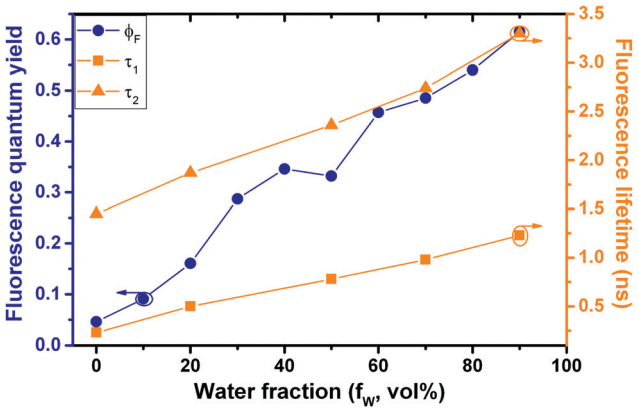

Fig. 5 Correlation of fluorescence quantum yields and fluorescence decay times for **Poly-*t*-Bu** in THF:water mixtures with increasing water fraction (f_W).

The decay time values together with the fractional contribution of each species (C_i) at the aggregate emission wavelength (525 nm) change with the increase of the water fraction in the mixture (Fig. 5). For **Poly-*t*-Bu** in THF a fast decay component, τ_1, in the 0.23–1.2 ns range and a longer decay time, τ_2, ranging from 1.5 ns to 3.3 ns were found on going from 0% to 90% water content (Table 4). As shown in Fig. 5 the fluorescence quantum yields and the fluorescence lifetimes follow a similar trend, *i.e.*, a concomitant increase of these parameters with the increase of the water fraction. In addition, the determination of the radiative (k_F) and radiationless (k_{NR}) rate constants clearly shows a decrease of k_{NR} and an increase of k_F with f_W. This is valid for the two decay components, but in Table 4 the data are only shown for the longer (τ_2) component. The radiationless decay is therefore dominant up to f_W = 70%, and from there on the radiative deactivation begins to dominate.

Conclusions

In summary, in this work we have synthesized propeller-shaped structures derived from tetraphenylethylene (**TPE**). The optical and PL properties of these compounds were studied in the solid state (powder and films) and in solution (THF and THF:water mixtures). Their properties were compared to the model compound **TPE** in similar experimental conditions. **Mono-*t*-Bu** and **Mono-Np**, monomeric model compounds with *para*-position *tert*-butyl substituents and naphthalene-substituted ethenes, respectively, showed AIE active properties in the solid state and in THF:water mixtures. This behavior is attributed to RIR in the solid state and when the compounds aggregate with the addition of the "poor solvent" (water), which hinders the excited state radiationless channels. The polymer **Poly-*t*-Bu** was found to be more fluorescent than its monomer **Mono-*t*-Bu** and to retain its AIE active properties. The ϕ_F value of **Poly-*t*-Bu** is found to be one order of magnitude higher in the solid state than in solution (ϕ_F = 64% in film *vs.* 4.6% in THF). This is accompanied by distinct microporosity in the solid state with a high S_{BET} surface area of 417 m^2 g^{-1}, probably driven by the steric demand of the *tert*-butyl groups. **Poly-*t*-Bu**, therefore, represents a so-called conjugated polymer of intrinsic microporosity (cPIM) with an attractive combination of intrinsic microporosity and occurrence of distinct AIE effects, thus predestining further experiments into stimuli-responsive properties in contact with suited analytes. In contrast, the diphenyl-dinaphthylethylene derivative polymers, **Poly-Np1** and **Poly-Np2**, are less emissive than **Mono-Np** and presented ACQ properties. These properties are assigned to the occurrence of strong π–π interactions in these polymers, leading to the formation of non-fluorescent H-aggregates. The occurrence of π–π interactions may also lead to tight packing of **Poly-Np1** and **Poly-Np2**, since these polymers do not show intrinsic microporosity (S_{BET} < 17 m^2 g^{-1}).

Conflicts of interest

There are no conflicts to declare.

Acknowledgements

This work was supported by Project "Hylight" (no. 031625) 02/SAICT/2017 which is funded by the Portuguese Science Foundation and Compete Centro 2020. We acknowledge funding from Fundo Europeu de Desenvolvimento Regional (FEDER) through Programa Operacional Factores de Competitividade (COMPETE) and project ROTEIRO/0152/2013. The Coimbra Chemistry Centre is supported by the Fundacão para a Ciência e a Tecnologia (FCT), Portuguese Agency for Scientific Research, through the Project PEst-OE/QUI/UI0313/2014. The research leading to these results has received funding from Laserlab-Europe (grant agreement no. 284464, EC's Seventh Framework Programme).

Notes and references

1 Y. Tang and B. Z. Tang, *Principles and Applications of Aggregation-Induced Emission*, Springer International Publishing, *Cham*, 2019.
2 Y. Hong, J. W. Lam and B. Z. Tang, *Chem. Commun.*, 2009, 4332–4353, DOI: 10.1039/b904665h.
3 J. B. Birks, *Photophysics of Aromatic Molecules*, Wiley- Interscience, London, 1970.
4 S. Baysec, E. Preis, S. Allard and U. Scherf, *Macromol. Rapid Commun.*, 2016, **37**, 1802–1806.
5 J. Chen, C. C. W. Law, J. W. Y. Lam, Y. Dong, S. M. F. Lo, I. D. Williams, D. Zhu and B. Z. Tang, *Chem. Mater.*, 2003, **15**, 1535–1546.
6 W. Z. Yuan, Y. Gong, S. Chen, X. Y. Shen, J. W. Y. Lam, P. Lu, Y. Lu, Z. Wang, R. Hu, N. Xie, H. S. Kwok, Y. Zhang, J. Z. Sun and B. Z. Tang, *Chem. Mater.*, 2012, **24**, 1518–1528.
7 Y. Dong, J. W. Y. Lam, A. Qin, J. Liu, Z. Li, B. Z. Tang, J. Sun and H. S. Kwok, *Appl. Phys. Lett.*, 2007, **91**, 011111.
8 X. Du, J. Qi, Z. Zhang, D. Ma and Z. Y. Wang, *Chem. Mater.*, 2012, **24**, 2178–2185.
9 S. Biswas, D. Jana, G. S. Kumar, S. Maji, P. Kundu, U. K. Ghorai, R. P. Giri, B. Das, N. Chattopadhyay, B. K. Ghorai and S. Acharya, *ACS Appl. Mater. Interfaces*, 2018, **10**, 17409–17418.
10 J. Huang, Y. Jiang, J. Yang, R. Tang, N. Xie, Q. Li, H. S. Kwok, B. Z. Tang and Z. Li, *J. Mater. Chem. C*, 2014, **2**, 2028–2036.
11 G. Liang, J. W. Y. Lam, W. Qin, J. Li, N. Xie and B. Z. Tang, *Chem. Commun.*, 2014, **50**, 1725–1727.
12 M. H. Chua, H. Zhou, T. T. Lin, J. Wu and J. Xu, *ACS Omega*, 2018, **3**, 16424–16435.
13 J. M. Hoyt and C. E. Frank, *US Pat.*, 3345332, Apr. 2, 1964, patented Oct. 3, 1967.
14 H. H. Hörhold and D. Raabe, *Acta Polym.*, 1979, **30**, 86–92.
15 H. Reisch, U. Wiesler, U. Scherf and N. Tuytuylkov, *Macromolecules*, 1996, **29**, 8204–8210.
16 E. Preis and U. Scherf, *Macromol. Rapid Commun.*, 2006, **27**, 1105–1109.
17 W. J. Feast and I. S. Millichamp, *Polym. Commun.*, 1983, **24**, 102–103.
18 C. Belton, D. F. O'Brien, W. J. Blau, A. J. Cadby, P. A. Lane, D. D. C. Bradley, H. J. Byrne, R. Stockmann and H. H. Hörhold, *Appl. Phys. Lett.*, 2001, **78**, 1059–1061.
19 Q. Chen, J.-X. Wang, F. Yang, D. Zhou, N. Bian, X.-J. Zhang, C.-G. Yan and B.-H. Han, *J. Mater. Chem.*, 2011, **21**, 13554–13560.
20 Y. Xu, L. Chen, Z. Guo, A. Nagai and D. Jiang, *J. Am. Chem. Soc.*, 2011, **133**, 17622–17625.
21 S. Dalapati, C. Gu and D. Jiang, *Small*, 2016, **12**, 6513–6527.
22 J. C. Jansen, E. Esposito, A. Fuoco and M. Carta, *Polymers*, 2019, **11**, 844, DOI: 10.3390/polym11050844.
23 G. Cheng, B. Bonillo, R. S. Sprick, D. J. Adams, T. Hasell and A. I. Cooper, *Adv. Funct. Mater.*, 2014, **24**, 5219–5224.
24 A. Palma-Cando, D. Woitassek, G. Brunklaus and U. Scherf, *Mater. Chem. Front.*, 2017, **1**, 1118–1124.
25 V. S. Mothika, A. Räupke, K. O. Brinkmann, T. Riedl, G. Brunklaus and U. Scherf, *ACS Appl. Nano Mater.*, 2018, **1**, 6483–6492.
26 Y. Xu, S. Jin, H. Xu, A. Nagai and D. Jiang, *Chem. Soc. Rev.*, 2013, **42**, 8012–8031.
27 A. Patra and U. Scherf, *Chem. – Eur. J.*, 2012, **18**, 10074–10080.
28 D. Chen, C. Liu, J. Tang, L. Luo and G. Yu, *Polym. Chem.*, 2019, **10**, 1168–1181.
29 G. M. Sheldrick, *Acta Crystallogr., Sect. A: Found. Adv.*, 2015, **71**, 3–8.
30 G. M. Sheldrick, *Acta Crystallogr., Sect. C: Struct. Chem.*, 2015, **71**, 3–8.
31 O. V. Dolomanov, L. J. Bourhis, R. J. Gildea, J. A. K. Howard and H. Puschmann, *J. Appl. Crystallogr.*, 2009, **42**, 339–341.
32 J. Pina, J. S. D. Melo, H. D. Burrows, A. Bilge, T. Farrell, M. Forster and U. Scherf, *J. Phys. Chem. B*, 2006, **110**, 15100–15106.
33 D. P. Law, A. B. Blakeney and R. Tkachuk, *J. Near Infrared Spectrosc.*, 1996, **4**, 189–193.
34 G. Striker, V. Subramaniam, C. A. M. Seidel and A. Volkmer, *J. Phys. Chem. B*, 2002, **103**, 8612–8617.
35 C. Gao, J. Y. Seow, B. Zhang, C. R. Hall, A. J. Tilley, J. M. White, T. A. Smith and W. W. H. Wong, *ChemPlusChem*, 2019, 746–753, DOI: 10.1002/cplu.201900100.
36 F. De Nisi, R. Francischello, A. Battisti, A. Panniello, E. Fanizza, M. Striccoli, X. Gu, N. L. C. Leung, B. Z. Tang and A. Pucci, *Mater. Chem. Front.*, 2017, **1**, 1406–1412.
37 J. Zhou, Z. Chang, Y. Jiang, B. He, M. Du, P. Lu, Y. Hong, H. S. Kwok, A. Qin, H. Qiu, Z. Zhao and B. Z. Tang, *Chem. Commun.*, 2013, **49**, 2491–2493.
38 H.-H. Hörhold, J. Gottschaldt and J. Opfermann, *J. Prakt. Chem.*, 1977, **319**, 611–621.
39 H.-H. Hörhold, M. Helbig, D. Raabe, J. Opfermann, U. Scherf, R. Stockmann and D. Weiß, *Z. Chem.*, 1987, **27**, 126–137.
40 S. Gonzalez, R. Pelaez, F. Sanz, M. B. Jimenez, J. R. Moran and M. C. Caballero, *Org. Lett.*, 2006, **8**, 4679–4682.
41 D. Sek, *Polym. J.*, 1981, **13**, 13–22.
42 C. Friedel and J. Crafts, *C. R. Chim.*, 1877, **84**, 1392–1396.
43 T. Mukaiyama, T. Sato and J. Hanna, *Chem. Lett.*, 1973, 1041–1044.
44 A. C. B. Rodrigues, J. Pina, W. Dong, M. Forster, U. Scherf and J. S. S. D. Melo, *Macromolecules*, 2018, **51**, 8501–8512.
45 W. Tian, T. Lin, H. Chen and W. Wang, *ACS Appl. Mater. Interfaces*, 2019, **11**, 6302–6314.
46 G. F. Zhang, Z. Q. Chen, M. P. Aldred, Z. Hu, T. Chen, Z. Huang, X. Meng and M. Q. Zhu, *Chem. Commun.*, 2014, **50**, 12058–12060.
47 J. Mei, Y. Hong, J. W. Y. Lam, A. Qin, Y. Tang and B. Z. Tang, *Adv. Mater.*, 2014, **26**, 5429–5479.
48 B.-K. An, S.-K. Kwon, S.-D. Jung and S. Y. Park, *J. Am. Chem. Soc.*, 2002, **124**, 14410–14415.
49 H. Zhang, J. Liu, L. Du, C. Ma, N. L. C. Leung, Y. Niu, A. Qin, J. Sun, Q. Peng, H. H. Y. Sung, I. D. Williams, R. T. K. Kwok, J. W. Y. Lam, K. S. Wong, D. L. Phillips and B. Z. Tang, *Mater. Chem. Front.*, 2019, 1143–1150, DOI: 10.1039/c9qm00156e,.
50 G. Tian, D. Sun, Y. Zhang and X. Yu, *Angew. Chem., Int. Ed.*, 2019, **58**, 5951–5955.

51 J. Mei, N. L. C. Leung, R. T. K. Kwok, J. W. Y. Lam and B. Z. Tang, *Chem. Rev.*, 2015, **115**, 11718–11940.
52 Y. Cai, L. Du, K. Samedov, X. Gu, F. Qi, H. H. Y. Sung, B. O. Patrick, Z. Yan, X. Jiang, H. Zhang, J. W. Y. Lam, I. D. Williams, D. Lee Phillips, A. Qin and B. Z. Tang, *Chem. Sci.*, 2018, **9**, 4662–4670.
53 Z. Qiu, X. Liu, J. W. Y. Lam and B. Z. Tang, *Macromol. Rapid Commun.*, 2019, **40**, 1–15.
54 E. Preis, W. Dong, G. Brunklaus and U. Scherf, *J. Mater. Chem. C*, 2015, **3**, 1582–1587.
55 C. Gu, N. Huang, Y. Wu, H. Xu and D. Jiang, *Angew. Chem., Int. Ed.*, 2015, **54**, 11540–11544.
56 C. S. de Castro, T. F. G. G. Cova, A. C. C. Pais, D. Pinheiro, C. Nuñez, C. Lodeiro and J. S. Seixas de Melo, *Dyes Pigm.*, 2016, **134**, 601–612.